ARTICLES

Effects of Geometry and Composition on Charge-Induced Plasmonic Shifts in Gold Nanoparticles

Bala Krishna Juluri,[†] **Yue Bing Zheng,**[†] **Daniel Ahmed,**[†] **Lasse Jensen,**[‡] **and Tony Jun Huang*,**[†]

Department of Engineering Science and Mechanics and Department of Chemistry, The Pennsylvania State University, University Park, Pennsylvania 16802

Received: September 12, 2007; In Final Form: January 9, 2008

In this work the influence of geometry and composition on the charge-induced plasmonic shifts (CIPS) of gold nanoparticles are systematically studied using Mie scattering theory and the discrete dipole approximation. The sensitivity of nanorods and nanodisks with different aspect ratio and nanoshells with different volume fractions and compositions are studied using different charging levels. The electrodynamics calculations were performed by changing the internal electron density in the Drude model for the dielectric constant of gold. We show that, for a constant volume, nanodisks and nanorods exhibit CIPS with a linear dependence on aspect ratio. Geometries having higher aspect ratio show larger CIPS. In nanoshells, increasing the volume fraction of the core causes a slow increase of CIPS at first followed by a rapid increase for larger volume fractions. In addition, we find that nanoshells with the same volume fractions exhibit larger shifts when the refractive index of the cores is larger. Furthermore, the electrodynamics results are interpreted using analytical approximations based on quasistatic theory. The qualitative understanding of geometric and composition effects on the CIPS of gold nanoparticles obtained in this work can hopefully be used to realize highly tunable charge-based active plasmonic devices.

I. Introduction

The phenomena of scattering and absorption of localized surface plasmons by nanometer-sized, noble metal particles have gathered much research interest in the past two decades. Key applications of these phenomena include biosensing,[1,2] contrast-enhanced imaging,[3,4] and optoelectronic devices.[5] Many of these applications involve active tuning of the resonance positions, which can be achieved by changing the following parameters: the size and shape of the particles,[6–9] the inter-particle distance,[7,10,11] the dielectric constant of the surrounding medium,[9,12–15] and the particles free electron density.[16–22]

Charge-induced plasmonic shifts (CIPS) of extinction spectra due to changes in the free electron density of gold and silver nanoparticles have been demonstrated in recent years. Nanoparticles in a colloid or immobilized on a substrate were charged either by adding a reducing agent or by applying an electrochemical potential. For an applied electrochemical potential, the amount of charge or discharge or the number of electrons transferring in or out of the nanoparticle was proportional to the double-layer capacitance across the solid–liquid interface. The direction of the shift was controlled by the electrochemical polarization and the amount of charge injection was limited only by the evolution of hydrogen or oxidation of the solvent at higher potentials. An increase in internal free electron density caused a blueshift of the extinction spectra, while a decrease caused a redshift.[19,20] Ung et al.[19] controlled the resonance position of colloidal silver by electrochemical processes. Based on the observed spectral shifts, they reported a charge density change of 6.2%/V/particle. Chapman et al.[20] and Daniels et al.[23] have demonstrated CIPS in silver nanoparticles immobilized on an indium tin oxide (ITO) substrate. Similar work was performed by Baum et al.[22] on gold nanospheres adsorbed on ITO. Gold nanospheres were immobilized by Toyota et al.[21] with an amine-terminated, siloxane-linking monolayer. This configuration was used to study the effects of both constant and modulated potential on the transmission and absorption properties of the nanoparticles. All of these studies were performed with nanoparticles of spherical shape and concluded that changes in free electron density alter the optical constants of the nanoparticles and thus the resonance positions.

In recent years, the increase of research in plasmonic applications has led to the synthesis of new nanoparticle geometries. Wet chemistry has been used to synthesize nanoparticle geometries such as nanorods,[24–26] nanodisks,[27] nanoshells,[28,29] hexagonal prisms,[30] etc. On the other hand, certain applications of plasmonics which require a supporting substrate have led to the fabrication of nanoparticles on the substrate using electron beam lithography[31–33] and colloidal lithography.[34,35] In these methods, arrays of nanoparticle geometries like nanodisks,[13,36] nanotriangles,[34,37,12] nanorings,[35,38] nanoprisms,[39] etc. are directly fabricated on a substrate, resulting in a more uniform and controlled distribution of nanoparticles unlike the monolayer linking of nanoparticles synthesized by wet chemistry. Moreover nanoparticles fabricated by colloidal lithography are extremely

* Corresponding author. E-mail: junhuang@psu.edu. Tel: (+1) 814 863 4209. Fax: (+1) 814 865 9974.
† Department of Engineering Science and Mechanics.
‡ Department of Chemistry.

7310 *J. Phys. Chem. C, Vol. 112, No. 19, 2008*

Juluri et al.

stable to positive potentials applied on the ITO surface.[40] We believe that the resonance position in new geometries fabricated both by the bottom-up and top-down methods can be tuned by charging and discharging.

Recently, Mulvaney et al.[41] have experimentally demonstrated that gold nanorods exhibit drastic blueshifts in optical resonance position when their free electron density increases. They also showed that CIPS strongly depends on the nanorod aspect ratio (AR). Geometries such as nanodisks, nanorods, and nanoshells can be tailored to obtain the desired CIPS. CIPS in these new geometries will find applications in building electrochemically tunable nanophotonic devices such as electrochromic devices and active waveguides. CIPS can also be potentially used to detect redox activity in the vicinity of nanoparticles and should find applications in sensing. Realizing these applications entails the understanding of optical effects of charging and its dependence on geometry and composition of nanoparticles.

In this direction, we report the effects of electron charging on both composite (hollow and solid nanoshells) and nonspherical nanoparticle geometries (nanodisks and nanorods) using electrodynamic simulations. Based on plasmonic shifts, comparison of these geometries, and influence of AR, volume fraction (VF) and composition within specific geometries are presented systematically for different levels of charging. Furthermore, the calculated CIPS sensitivities of various nanoparticle geometries and compositions are rationalized in terms of approximate analytical expressions based on quasistatic theory. It is shown that the CIPS sensitivity of nanoparticle is significantly affected by the AR and composition of the nanoparticle, and should be taken into account to maximize the nanoparticle CIPS sensitivity.

Section II outlines the various theoretical methods to calculate CIPS in nanoparticles. Section III presents the electrodynamic results for various geometries and compositions and the analytical expressions based on quasistatic theory to correlate with results obtained from the electrodynamic methods. Finally, section IV concludes this work.

II. Theory

The extinction efficiency of nanoparticles can be numerically calculated by various methods, which include Mie scattering theory (MST),[42] discrete dipole approximation method (DDA),[43] T-matrix method,[44] modified long wavelength approximation (MLWA),[43] and finite difference time domain method (FDTD).[33,45] In this work, we used DDA for nanodisks and nanorods, and MST for hollow and solid nanoshells to calculate the resonance positions ($\lambda_{\Delta N}$ and λ_0) for both charged and uncharged states. CIPS is calculated as the difference between these two wavelengths, $\Delta\lambda = \lambda_0 - \lambda_{\Delta N}$. To remove the effect of particle size on CIPS, the volume of all of the nanoparticles was kept constant and an effective spherical radius (r_{eff}) of 10 nm was chosen. The surrounding environment of all isolated nanoparticles was considered to be water with an refractive index (RI) of 1.333, as charging is generally performed in aqueous environment (double layer capacitance in water is higher than in air).

A. Drude Model. An increase in free electron density affects the dielectric constant of the Au nanoparticles. To calculate the extinction spectra for various particle geometries in charged and uncharged states, we have considered a Drude-type dielectric function in DDA and MST. The generalized Drude model does not account for the effects of size and shape on the particles' dielectric constants. We modeled the nanoparticles with an effective radius equal to 10 nm, large enough to neglect size

and shape effects in the Drude model.[7] As the size of the particles used in previously reported CIPS experiments is less than 50 nm, we restrict our studies to particles with sizes below 50 nm. In this size regime, the effect of retardation and damping are negligible[6,46] and variations in size will only affect the line width of the spectrum.[29] In this work we are mainly interested in the changes in location of the resonance wavelength.

The analytic expressions for the Drude model with these considerations are[6]

$$\epsilon(\omega^3) = \epsilon'(\omega^3) + i\epsilon''(\omega^3) = \epsilon_\infty - \frac{\omega_p^2}{\omega^2 + i\gamma\omega} \tag{1}$$

$$\epsilon'(\omega) = \epsilon_\infty - \frac{\omega_p^2}{\omega^2 + \gamma^2} \tag{2}$$

and

$$\epsilon''(\omega) = \frac{\gamma\omega_p^2}{\omega^3 + \gamma^2\omega} \tag{3}$$

where ϵ' is the real part of the dielectric function, ϵ'' is the imaginary part of the dielectric function, ϵ_∞ is the contribution from the bound electrons, ω_P is the bulk plasma frequency ($\omega_P^2 = Ne^2/\epsilon_0 m^*$), and γ is the relaxation constant such that $\gamma = Ne^2/\sigma m^*$ where, N is the free electron density, e is the charge of an electron, m^* is the effective mass of an electron, and σ is the conductivity. It should be noted that ω_P is a function of free electron density (N), whereas the relaxation constant is independent of N as the conductivity is also proportional to N. It is therefore expected that any change in free electron density will change the resonance position via ω_P. When the internal free electron density is increased by ΔN, the real and imaginary parts of the dielectric function are given by

$$\epsilon'_{\Delta N}(\omega) = \epsilon_\infty - \frac{\omega_p^2(1 + \Delta N/N)}{\omega^2 + \gamma^2} \tag{4}$$

and

$$\epsilon''_{\Delta N}(\omega) = \frac{\gamma\omega_p^2(1 + \Delta N/N)}{\omega^3 + \gamma^2\omega} \tag{5}$$

respectively.

Figure 1, panels a and b, shows the real and imaginary parts of the frequency-dependent dielectric constant of gold. The solid circles are the experimental results from Johnson et al.[47] The lines represent results from the Drude model for both uncharged and charged ($\Delta N/N = 14\%$) states. The parameters $\omega_P = 9$ eV, $\gamma = 67$ meV, and $\epsilon_\infty = 9.84$ were used to fit the experimental data with the above-mentioned Drude model and were obtained from the work by Sönnichsen.[46] The imaginary part of the dielectric constant for wavelengths below 700 nm cannot be properly fit with the Drude model due to the contributions from interband transitions.[46] As the resonance position is dependent primarily on the real part of the dielectric function, a proper fit of the real part is required to accurately calculate the resonance position. This requirement is satisfied by the Drude model for wavelengths higher than 500 nm (see Figure 1a). However, the peak intensity and width will be dependent on the imaginary part. In order to confirm this, we compared calculations using both the experimental dielectric data and the Drude model of uncharged particles exhibiting different plasmon resonance. The

CIPS in Au Nanoparticles

J. Phys. Chem. C, Vol. 112, No. 19, 2008 **7311**
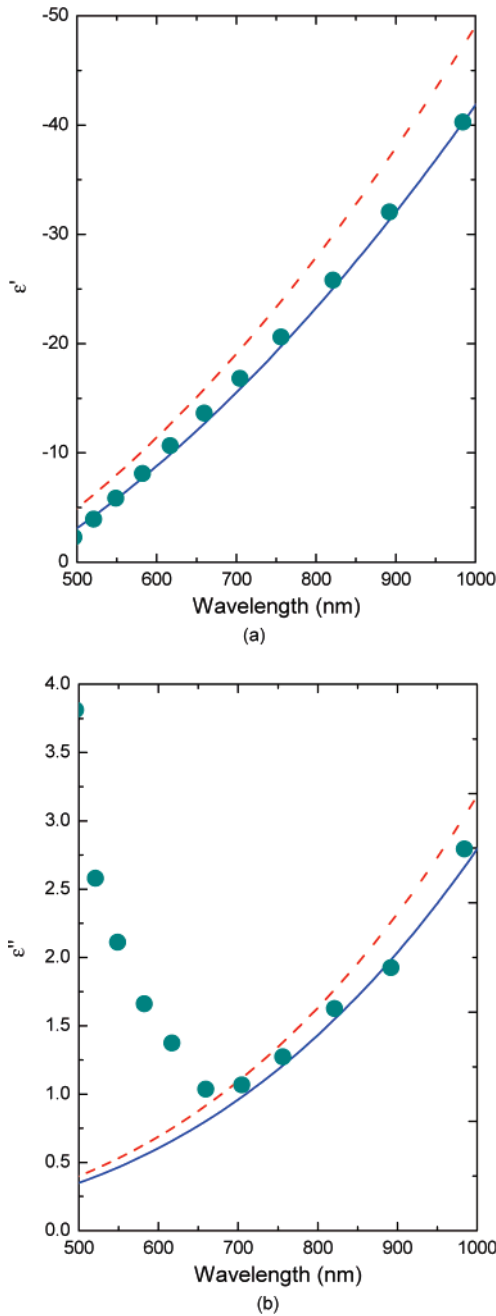
Figure 1. (a) Real and (b) imaginary parts of the frequency-dependent dielectric function of gold. Experimental data from Johnson et al.[47] (solid circles) and the fitted Drude model (parameters obtained from Sönnichsen et al.[46]) for uncharged state (solid line) and charged state with $\Delta N/N = 14\%$ (dotted line).

details can be found in the Supporting Information. Our results show that, although we are not able to accurately describe the extinction intensities and widths below 700 nm, the peak position can be modeled correctly for wavelengths above 500 nm. For plasmon resonance modes below 500 nm, the Drude dielectric function fails to predict the position of plasmon mode as the real part of the dielectric function deviates from the experimental data. Therefore, for wavelength above 500 nm the Drude model suffices to accurately describe the plasmon peak position. Since the amount of charge injected into nanoparticles can be varied by double-layer capacitance and applied electrochemical potential, we considered a wide range of charging levels ($\Delta N/N = [-7\%, +7\%, +14\%, +21\%]$) in the electrodynamics calculations.

B. Discrete Dipole Approximation (DDA). The discrete dipole approximation (DDA) method can be used to calculate the extinction properties of nanoparticles with arbitrary geometry and composition. It has been extensively employed in surface plasmon resonance calculations. DDA was first developed by Purcell and Pennpacker[48] and was later improved by Draine and Flauteu.[49,50] DDA calculates the extinction spectra by describing the particle shape as a collection of M dipoles arranged in cubic lattice such that each dipole responds to both the incident electric field and electric fields induced by neighboring dipoles. The polarization $\mathbf{P}_j$ of a dipole j is given by $\alpha_j \mathbf{E}_j$, where α_j is the polarizability and $\mathbf{E}_j$ is the sum of the incident electric field $\mathbf{E}_{\text{inc},j} = \mathbf{E}_0 e^{i\mathbf{k}\cdot\mathbf{r}_j}$ and the electric field arising from the $M - 1$ other dipoles. The total electric field of jth dipole is then given by

$$\alpha_j^{-1}\mathbf{P}_j = \mathbf{E}_j = \mathbf{E}_{\text{inc},j} - \sum_{l \neq j}^{M} A_{jl}\cdot\mathbf{P}_l \qquad (6)$$

where the electric field from the other $M - 1$ dipoles are given by

$$A_{jl}\cdot\mathbf{P}_l = \frac{e^{ik\mathbf{r}_{jl}}}{\mathbf{r}_{jl}^3}\left[k^2\mathbf{r}_{jl} \times (\mathbf{r}_{jl} \times \mathbf{P}_l) + \frac{1 - ik\mathbf{r}_{jl}}{\mathbf{r}_{jl}^2}\{\mathbf{r}_{jl}^2\mathbf{P}_l - 3\mathbf{r}_{jl}(\mathbf{r}_{jl}\cdot\mathbf{P}_l)\}\right] \qquad (7)$$

Polarizations vectors of each dipole were calculated by solving the $3M$ complex linear equations resulting from eq 6. In order to calculate these linear equations we used the DDSCAT program by Draine and Flauteu[50] which uses Fast Fourier transformations and complex conjugate methods[51] to calculate the polarization vectors for a large number of dipoles. These calculated polarizations and incident electric fields are used to calculate extinction cross-section of the nanoparticle based on the optical theorem given by[42]

$$C_{\text{ext}}(\lambda) = \frac{4\pi k}{|\mathbf{E}_0|^2}\sum_{l=1}^{M}\text{Im}(\mathbf{E}_{\text{inc},l}^*\cdot\mathbf{P}_l) \qquad (8)$$

where k is the wave vector equal to $2\pi m/\lambda$ and m is the RI of the particle relative to the medium at wavelength λ. The extinction cross-section is normalized as the extinction efficiency, $Q_{\text{ext}} = C_{\text{ext}}/C_{\text{geom}}$, where the extinction cross-section is divided by the cross-section of a sphere with effective area $C_{\text{geom}} = \pi r_{\text{eff}}^2$. In this work, the lattice constant of 1 nm was taken for nanodisk and nanorod calculations to ensure accurate extinction spectra.[52]

C. Mie Scattering Theory (MST). Calculations based on Mie scattering theory (MST) are used to investigate the extinction spectra of hollow and solid nanoshells due to the capability of MST in obtaining the exact full solution to Maxwell's equation for the spherical nanoshells. This method involves solving Maxwell's equations in spherical coordinates with appropriate boundary conditions. According to MST, the extinction cross-section of core−shell structure is given by

$$C_{\text{ext}} = \frac{2\pi}{|k|^2}\sum_{n=1}^{\infty}(2n + 1)Re(a_n + b_n) \qquad (9)$$

where the scattering coefficients a_n and b_n are given by

$$a_n =$$
$$\frac{\psi_n(y) - m_2\psi'_n(y)[\psi_n(m_2y) - A_n\chi_n(m_2y)/\psi'_n(m_2y) - A_n\chi'_n(m_2y)]}{\xi_n(y) - m_2\xi'_n(y)[\psi_n(m_2y) - A_n\chi_n(m_2y)/\psi'_n(m_2y) - A_n\chi'_n(m_2y)]}$$
$$(10)$$

and

$$b_n =$$
$$\frac{m_2\psi_n(y) - \psi'_n(y)[\psi_n(m_2y) - B_n\chi_n(m_2y)/\psi'_n(m_2y) - B_n\chi'_n(m_2y)]}{m_2\xi_n(y) - \xi'_n(y)[\psi_n(m_2y) - B_n\chi_n(m_2y)/\psi'_n(m_2y) - B_n\chi'_n(m_2y)]}$$
$$(11)$$

respectively. In these scattering coefficients, ψ_n, ξ_n, and χ_n are the Riccati-Bessel functions and A_n and B_n are given by

$$A_n = \frac{m_2\psi_n(m_2x)\psi'_n(m_1x) - m_1\psi'_n(m_2x)\psi_n(m_1x)}{m_2\chi_n(m_2x)\psi'_n(m_1x) - m_1\chi'_n(m_2x)\psi_n(m_1x)} \quad (12)$$

and

$$B_n = \frac{m_2\psi_n(m_1x)\psi'_n(m_2x) - m_1\psi_n(m_2x)\psi'_n(m_1x)}{m_2\chi'_n(m_2x)\psi_n(m_1x) - m_1\psi'_n(m_1x)\chi_n(m_2x)} \quad (13)$$

respectively. m_1 and m_2 are the RI of the core and mantle relative to the surrounding dielectric medium, and $x = kr_{core}$ and $y = kr_{mantle}$ are wavenumbers of the core and mantle respectively. These calculated extinction cross-section are normalized as the extinction efficiency $Q_{ext} = C_{ext}/C_{geom}$. In this work, a Fortran code (bhcoat.f) presented by Bohren and Hauffman[42] was used to calculate the extinction spectra of nanoshells.

III. Results and Discussion

A. Nanorods and Nanodisks. The geometry, in particular AR, has been one of the most important parameters in determining the plasmonic resonance of metal nanorods and nanodisks.[15,26,53] In order to study the effects of geometry on CIPS in nanorods and nanodisks, we considered various ARs but maintained a constant volume. The AR of nanodisks in this work is defined as the ratio of diameter to height, and for nanorods it is defined as the ratio of length to diameter. Further, for each nanorod or nanodisk of specific AR, the influence of polarization of incident light on the CIPS is considered. When nanorods are suspended in solution, two types of polarization modes can be excited by linearly polarized or natural light. If the incident light has the electric field parallel to the longitudinal axis of nanorods, longitudinal plasmon mode is excited, and if the electric field is perpendicular to longitudinal axis, transverse modes get excited. Similarly in nanodisks, two types of modes, i.e., in-plane and out-of-plane modes, can be excited by controlling alignment between polarization of incident light and disk plane. In the in-plane polarization mode, the incident light direction is normal to the disk plane and the electric field is parallel to the diameter axis, whereas in the out-of-plane mode, the incident light direction is parallel to the disk plane and electric field perpendicular to the diameter axis.

Figure 2a illustrates the uncharged and charged state extinction spectra of two types of nanodisks with ARs of 2.5 and 4.5, respectively. These spectra were obtained by in-plane polarized incident light. In Figure 2a the uncharged state's peak resonance wavelength (λ_0) for nanodisks with AR = 4.5 is larger than that of AR = 2.5. Both nanodisks' peak positions blueshift upon charging ($\Delta N/N$ = 14%). In Figure 2b, we compare the uncharged and charged state spectra of nanorods of two different
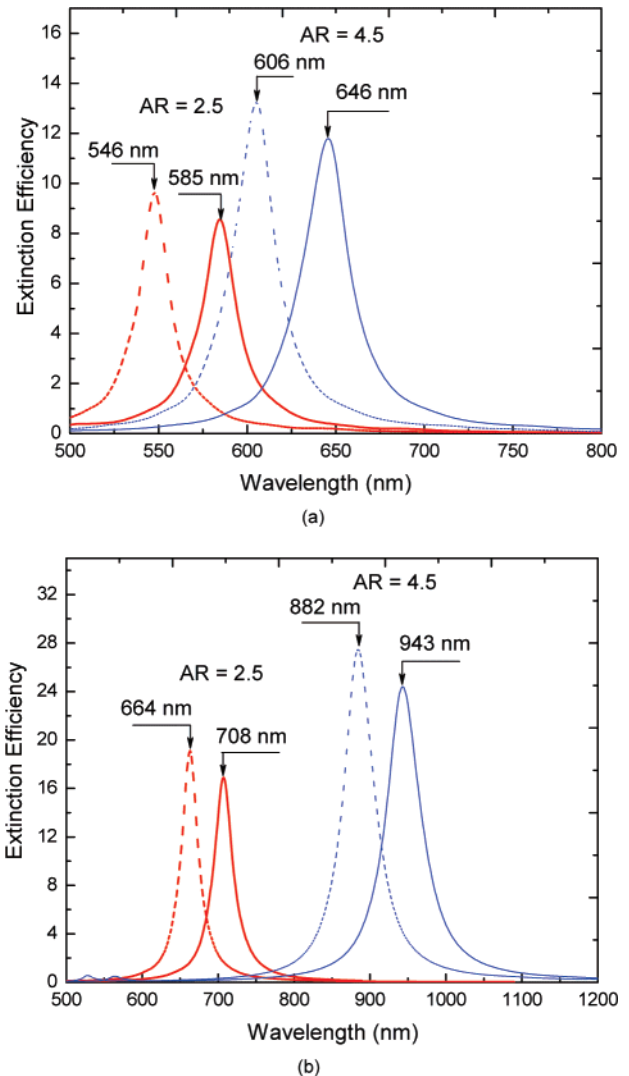
Figure 2. Extinction spectra of (a) in-plane polarization mode of nanodisks and (b) longitudinal polarization mode of nanorods at constant $r_{eff} = 10$ nm of ARs, 2.5 (thick lines) and 4.5 (thin lines) for uncharged state (solid lines) and charged states, $\Delta N/N = 14\%$ (dotted lines).

ARs, 2.5 and 4.5, when subjected to longitudinal polarized incident light. When the volume is held constant, nanorods of AR = 4.5 exhibit an uncharged state peak resonance wavelength near the infrared region, whereas nanodisks at the same AR are in the range of visible light. Similar to the nanodisks, the nanorods' spectra blue shifts upon electron charging. Figure 2, panels a and b, thereby show that the CIPS in nanodisks and nanorods are dependent on their ARs.

To quantitatively evaluate the relation between CIPS and AR of nanorods and nanodisks, our electrodynamics calculations included a fixed charge injection ($\Delta N/N = 14\%$) for various AR configurations. For each AR, different polarizations of incident light were also considered in order to understand the effects of polarization on CIPS. These results are summarized in Figure 3a, where the blueshifts of plasmonic resonance for various geometries and polarizations are plotted against the AR of the nanoparticles.

The CIPS due to the transverse polarizations in the nanorods and out-of-plane polarizations in the nanodisks remains almost constant as shown in Figure 3a. It should be noted that for certain ARs the transverse modes in nanorods and out-of-plane modes in nanodisks fall below 500 nm and, therefore, could

CIPS in Au Nanoparticles

J. Phys. Chem. C, Vol. 112, No. 19, 2008 **7313**
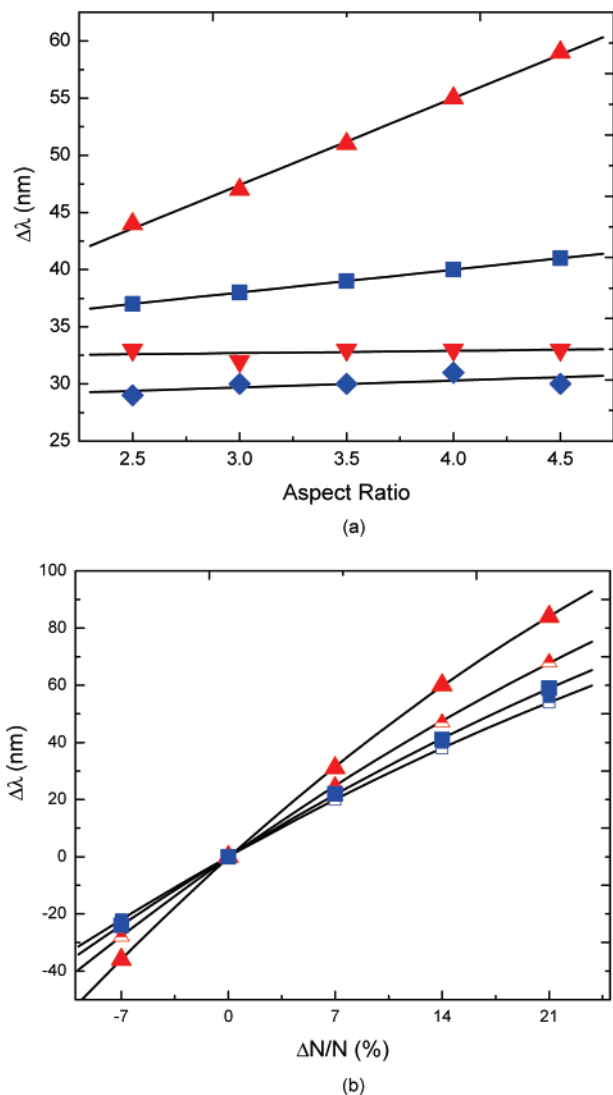
Figure 3. (a) Calculated CIPS for $\Delta N/N = 14\%$ and various nanorod ARs, longitudinal modes (triangles) and transverse modes (inverted triangles); in nanodisks, in-plane mode (squares) and out-of plane mode (diamonds). (b) Longer wavelength plasmonic mode CIPS for various charging levels, nanorods with AR = 4.5 (triangles) and 2.5 (half filled triangles); nanodisks with AR = 4.5 (squares) and 2.5 (half filled squares). Solid lines are best fits.

Figure 4. Extinction spectra of (a) hollow nanoshells and (b) solid nanoshells at constant $r_{eff} = 10$ nm; radius ratios are 0.8 (thick lines) and 0.95 (thin lines) for the uncharged state (solid lines); and for the charged states (dotted lines), $\Delta N/N = 14\%$. The two peaks at a certain charge state and volume fraction represent two different energy plasmonic resonances.

not be calculated accurately with the Drude dielectric function. However, it is likely that the CIPS is less dependent on the dielectric function than the peak position itself since the CIPS is almost constant for all ARs. In contrast, the longitudinal polarization of nanorods and the in-plane polarization of nanodisks result in larger CIPS, which follows an increasing linear dependence on AR. From the slopes of linear fits in Figure 3a, we observe that at a certain charging level, AR and volume, nanorods exhibit more CIPS than nanodisks; this difference in CIPS increases with AR. To further evaluate the effects of charging on the CIPS, we calculated the shifts of the longer wavelength plasmonic mode resonances (in-plane polarization mode in nanodisks and longitudinal polarization mode in nanorods) by considering different levels of charging. Figure 3b shows the effect of charging level on CIPS calculated for nanodisks and nanorods with two different ARs, 2.5 and 4.5. From Figure 3b, we can observe that, for both nanorods and nanodisks, CIPS at a particular AR follows a linear relationship at lower charging levels and this linear behavior deviates at higher charging levels. For a range of charging levels and

constant volumes, geometries with higher AR result in larger plasmonic shifts, and CIPS in nanorods is larger than that in nanodisks.

B. Hollow and Solid Nanoshells. Metal nanoshells have attracted tremendous interest for their ability to obtain plasmonic resonance over a large range by controlling the shell thickness or core compositions.[29,2] To understand the effect of shell composition on CIPS, we carried out a series of electrodynamic calculations using MST on hollow and solid shells. The RI of the hollow shells core was taken to be equal to the surrounding environment (water), while the RI of the solid shell was varied from 1.333 to 2.332. To understand the effect of VF on plasmonic shifts, different ratios R_c/R_m (the core radius, R_c, divided by the total radius, R_m, of the core−shell particle) were considered. This ratio of the nanoshells can be engineered and nanoshells with ratios between 0.33 and 0.92 have been fabricated and studied perviously.[54]

Figure 4, panels a and b, shows the uncharged and charged state ($\Delta N/N = 14\%$) spectra of hollow and solid nanoshells (RI

(a)

(b)
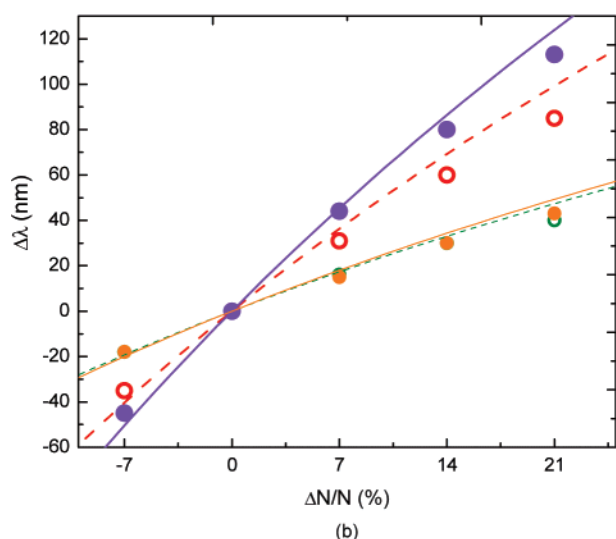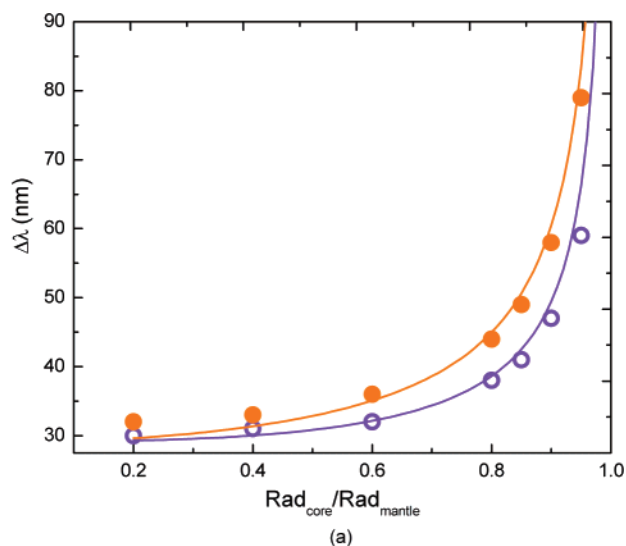
Figure 5. CIPS of longer wavelength plasmon mode in nanoshells, by MST calculation (discrete points) and by eqs 25 and 27 based on quasistatic theory (lines) for a) charging ($\Delta N/N = 14\%$) different radius ratios (0.2–0.95), hollow nanoshells (hollow circles) and solid nanoshells with core RI = 2.332 (solid circles); (b) different amounts of charging ($\Delta N/N$) = −7% to +21%) at constant $r_{eff} = 10$ nm, in hollow nanoshells with different radius ratios (0.6, the smaller hollow circles; 0.95, the larger hollow circles) as well as solid nanoshells with different radius ratios (0.6, the smaller solid circles; 0.95, the larger solid circles).

= 2.332) with different VFs. Two peaks (one at a wavelength below 500 nm and the other above 500 nm) are observed for each charged state, representing two different plasmon modes. As mentioned previously the plasmon mode below 500 nm cannot be accurately calculated using the Drude dielectric function, and therefore, we will only describe the long wavelength plasmon modes. It can be seen that the peak resonance wavelength in both solid and hollow nanoshells at different VFs blueshift upon charging, a behavior similar to that of nanodisks and nanorods. It is also observed that the CIPS and the uncharged peak position (λ_0) in nanoshells depend on the composition and VF of the core.

To evaluate the dependence of CIPS on the VF of the core, a series of electrodynamic calculations using MST was performed with various VFs and the results are summarized in Figure 5a. The charge-induced plasmonic blueshift increases with increasing radius ratio between the core and the mantle. This increase is slow when the radius ratio is smaller than 0.7.
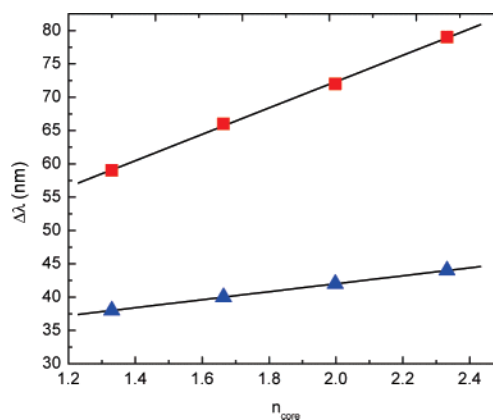
Figure 6. CIPS in solid nanoshells due to $\Delta N/N = 14\%$ charging for different core RIs, 1.333−2.332, and radius ratios, 0.6 (triangles) and 0.95 (squares). Solid lines are best fits made in order to understand the trends.

However, as the radius ratio reaches unity, rapid increasing in CIPS occurs. It can also be observed that solid nanoshells with core RI higher than hollow nanoshells result in larger shift at a particular radius ratio.

The effect of charging level and VF's on CIPS in both hollow and solid nanoshells is shown in Figure 5(b). Note that the lines in Figure 5, panels a and b, are not fits but correspond to the shifts predicted by quasistatic approximation described in the next section. CIPS at a particular RI and VF of the core follow a linear relationship with the amount of charging. This linear behavior deviates after a certain value of charging, similar to what was found for the nanodisks and nanorods. From Figure 5b, it can also be observed that a higher RI of the core in conjunction with a higher VF lead to larger CIPS over a range of charging levels. In addition, Figure 6 presents the dependence of plasmonic shifts on RI at different ARs. It can be seen that plasmonic shifts follow a linear relationship with the RI of the core. The slopes of the linear fits indicate that higher core VF causes larger CIPS in the nanoshells.

C. Quasistatic Theory Approximation. In comparison with the electrodynamics calculations presented above, analytic expressions provide an intuitive way to understand and interpret qualitative behavior of the plasmonic shifts. In this section we focus on quasistatic theory to understand the effects of geometry and composition on CIPS in nanoparticles. In quasistatic theory, the spatial variation of the electromagnetic field is neglected and only temporal variation is considered, with the aim of calculating an approximate peak resonance wavelength.[6] Mulvaney et al.[41] have used quasistatic theory and the Drude model to explain the dependence of nanorod AR on CIPS. In their work, as the charge injection was performed by reducing gold nanorods using $NaBH_4$ and also to simplify the formulation, they assumed that the amount of added internal free electron density is much smaller than the existing internal free electron density, ($\Delta N/N \ll 100\%$). As the amount of charge injected into the nanoparticles can be increased by applying a greater electrochemical potential or increasing the double-layer capacitance, we have considered higher levels of charging in our model. We also extend our investigation into various other nanoparticle geometries (nanodisks and nanoshells).

According to quasistatic theory, the polarizability of nanodisks and nanorods, when approximated as oblate and prolate spheroids, respectively, is given by[42]

CIPS in Au Nanoparticles

J. Phys. Chem. C, Vol. 112, No. 19, 2008 **7315**

$$\alpha_1 \propto \left(\frac{\epsilon_1 - n^2}{n^2 + L(\epsilon_1 - n^2)} \right) \qquad (14)$$

where ϵ_1 is the Drude type dielectric function of nanorods and nanodisks; n is the RI of the surrounding medium; and L is a geometry-dependent polarization factor for nanodisks and nanorods. The resonance condition corresponds to a wavelength at which the denominator of the polarizability equals to zero

$$\text{real}(n^2 + L(\epsilon_1 - n^2)) = 0 \qquad (15)$$

In the frequency range where ϵ'' is small or changes very slowly, ϵ_1 can be considered equal to ϵ'_1. Thus, the resonance condition is given by

$$\epsilon_1^{\text{reso}} = \left(1 - \frac{1}{L} \right) n^2 \qquad (16)$$

The polarizability of a solid shell, α_2, characterized by a core RI n_{core}, a mantle dielectric constant ϵ_2, a mantle VF P, and a surrounding RI n is given by[42]

$$\alpha_2 \propto \left(\frac{\epsilon_2 \epsilon_a - n^2 \epsilon_b}{\epsilon_2 \epsilon_a + 2n^2 \epsilon_b} \right) \qquad (17)$$

where

$$\epsilon_a = n_{\text{core}}^2 (3 - 2P) + 2\epsilon_2 P \qquad (18)$$

$$\epsilon_b = n_{\text{core}}^2 P + \epsilon_2 (3 - P) \qquad (19)$$

and

$$P = 1 - \left(\frac{R_c}{R_m} \right)^3 \qquad (20)$$

The poles of the polarizability expression are obtained from the denominator of eq 17 as

$$\text{real}[\epsilon_2 \epsilon_a + 2n^2 \epsilon_b] = 0 \qquad (21)$$

The resonance condition of solid nanoshells is therefore given by

$$\epsilon_2^{\text{reso}} = \frac{1}{4P} [-(n_{\text{core}}^2(3 - 2P) + 2n^2(3 - P)) \pm$$
$$\sqrt{(n_{\text{core}}^2(3 - 2P) + 2n^2(3 - P))^2 - 16P^2 n^2 n_{\text{core}}^2}] \quad (22)$$

In the case of hollow nanoshells, the RI of the core is equal to the surrounding RI, $n_{\text{core}} = n$. Upon incorporating this condition in eq 22, the resonance condition for hollow nanoshells is given by

$$\epsilon_3^{\text{reso}} = \frac{n^2}{4P} [-(9 - 4P) \pm 3\sqrt{9 - 8P}] \qquad (23)$$

The two solutions of resonance condition in nanoshells represent plasmon modes of two different energies and correlate with two peaks (one below 500 nm and other above 500 nm) observed in the extinction spectra shown in Figure 4, panels a and b. The two fundamental dipolar modes of core−shell nanoparticle can be thought to arise from the hybridization of a dipolar modes of the metallic sphere and a dielectric void in a metal substrate.[55]

The charged-state resonance wavelength ($\lambda_{\Delta N}$) is obtained by equating the charged-state dielectric constant of the nanoparticle

($\epsilon'_{\Delta N}$) to the dielectric constant at resonance (ϵ_i^{reso}). The charged-state dielectric constant of the nanoparticles is obtained from the real part of the Drude model as discussed in section 2.1

$$\epsilon_\infty - \frac{\omega_p^2(1 + \Delta N/N)}{\omega^2 + \gamma^2} = \epsilon_i^{\text{reso}} \quad i = 1{-}3 \qquad (24)$$

Substituting $\omega = c/\lambda_{\Delta N}$ and $\omega_p = c/\lambda_p$ in eq 24, we obtain an expression relating the resonance wavelength to the amount of charging, geometry and composition

$$\lambda_{\Delta N} = \frac{\lambda_p \sqrt{A_i}}{\sqrt{1 + (\Delta N/N) - (\gamma^2 A_i/\omega_p^2)}} \qquad (25)$$

where

$$A_i = \epsilon_\infty - \epsilon_i^{\text{reso}} \quad i = 1{-}3 \qquad (26)$$

The uncharged state resonance position (λ_0) is obtained by substituting $\Delta N = 0$ in eq 25

$$\lambda_0 = \frac{\lambda_p \sqrt{A_i}}{\sqrt{1 - (\gamma^2 A_i/\omega_p^2)}} \qquad (27)$$

Furthermore, the sensitivity of the nanoparticle, defined as the ratio of CIPS ($d\lambda = \lambda_0 - \lambda_{\Delta N}$) to the change in free electron density (dN) is obtained by subtracting eq 27 from eq 25 and dividing by the amount of charge injection.

$$\frac{d\lambda}{(dN/N)} = \frac{\lambda_0}{(\Delta N/N)} \left[\frac{\sqrt{1 - (\gamma^2 A_i/\omega_p^2)}}{\sqrt{1 + (\Delta N/N) - (\gamma^2 A_i/\omega_p^2)}} - 1 \right] \quad (28)$$

Equations 27 and 25 give the plasmonic shifts for various amounts of charging and various core VFs in solid and hollow nanoshells; the parameters A_2 and A_3 incorporate the effect of the core's VF and composition. CIPS of longer peak wavelength in nanoshells calculated based on quasistatic theory (eqs 27 and 25) and MST are shown in Figure 5, panels a and b, for solid and hollow nanoshells, respectively. This figure show the dependence of core VF and level of charging on the plasmonic shifts in nanoshells. In nanodisks and nanorods, the exact relationship between AR and L is unknown, but for shapes such as prolate and oblate spheroids, the exact relationship between AR and L is known and it is recognized in these shapes that higher ARs have lower L's. From eqs 16, 25, and 27, as AR increases or L decreases, the value of λ_0 increases as does the difference between λ_0 and $\lambda_{\Delta N}$. This behavior of higher CIPS at higher AR agrees with the electrodynamics calculations shown in Figure 3a. The combination of eqs 22, 25, and 27 demonstrates the dependence of CIPS in solid nanoshells on the RI of core and the VF. These equations rationalize the almost linear dependence of CIPS with the RI of core as observed in Figure 6.

Equation 28 estimates the plasmon shift sensitivity of a nanoparticle independent of its geometric parameters. The expression shows that the sensitivity is dependent only on the uncharged state resonance wavelength (λ_0) and the amount of charging (ΔN). Figure 7 presents the sensitivity of the plasmonic shift as a function of uncharged state resonance wavelength for all five geometries. Figure 7a compares the sensitivities of particles as calculated by DDA with analytic sensititivity expressions obtained from quasistatic theory. It can be observed
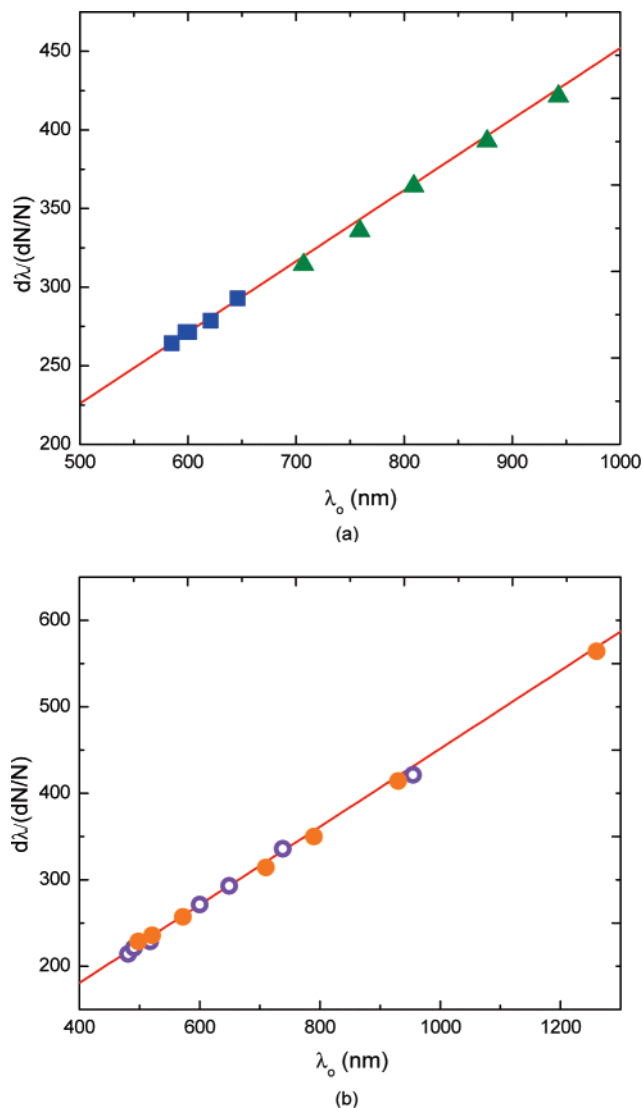
Figure 7. Dependence of CIPS sensitivity on uncharged optical resonance position (λ_0), electrodynamics calculations (discrete points) and by eq 28 based on quasistatic theory (line) at $\Delta N/N = 14\%$ for (a) nanodisks (squares) and nanorods (triangles) and (b) hollow (open circles) and solid nanoshells (solid circles).

that nanorods in general for comparable amounts of charging and volume are more sensitive than nanodisks due to the nanorods' higher uncharged state resonance wavelength. Figure 7b shows MST calculation results on nanoshells of various VFs and core RI, as well as a quasistatic analytical expression of sensitivity.

The expression for the plasmon shift sensitivity, eq 28, can be further simplified by assuming low levels of charging and neglecting the contributions from relaxation constant term. Using a binomial series expansion of the right-hand side of eq 28 and neglecting higher order terms, we obtain

$$\frac{d\lambda}{(dN/N)} \sim \frac{\lambda_0}{2} \qquad (29)$$

This equation indicates that the sensitivity of charging is approximately constant and is equal to half of the uncharged resonance position. A comparison with the results plotted in Figure 7 shows that this is a good approximation, although the results obtained using eq 28 predicts a slightly smaller sensitivity.

To develop nanoparticle-based devices with highly tunable CIPS, one must carefully design the particles' geometry and composition. As shown in Figure 7, panels a and b, lower energy or higher wavelength resonances result in higher sensitivities. The location of the extinction band in uncharged-state solid nanoparticles can be adjusted to obtain higher sensitivities. The adjustment in the band location can be achieved through changing the particles' shape or relative dimensions (such as AR). In composite structures, such as hollow and solid nanoshells, both geometrical variations and RI of the core can be engineered to lower the energy of the extinction wavelength.

The uncharged optical resonance position (λ_0) has been shown to redshift with an increase in the size of nanoshells and nanorods.[6,53] Therefore, CIPS sensitivity can be enhanced by increasing the size of the nanoparticle. But variations in double layer capacitance due to changes in size must be taken into account. Electrodynamics calculations in this study were performed assuming a constant RI of the surrounding environment. An increase in the surrounding environment's RI generally redshifts the resonance position.[12-15] Choosing a higher RI of the surrounding medium before charging would reduce the uncharged state's resonance energy and increase its CIPS sensitivity. A higher RI of the medium also increases the double layer capacitance of the nanoparticles, which increases the amount of charging per unit potential.

Nanodisks and nanorods fabricated on a substrate by top-down fabrications methods have the advantage of controllable polarization modes, unlike nanoparticles in colloids which have random polarization orientation. Control over polarization will lead to higher sensitivity. In our electrodynamics model, the nanoparticles were surrounded by a homogeneous medium (water). A substrate beneath the nanoparticles has a higher RI than the surrounding medium, and thus will cause a redshift of the resonance[6,56] and increase the CIPS sensitivity. Sensitivity can be further enhanced by applying a polymer film on top of the nanoparticles, because the polymer film increases the capacitance of the system.[20,57] In arrays of nanoparticles fabricated by nanosphere lithography, the interparticle distance should be optimized. Two effects should be considered for optimization: (1) dipole-coupling interactions between nanoparticles should be reduced to increase the CIPS sensitivity[20] and (2) the amount of charge injection should not be limited by charge induced Rayleigh instabilities.[58]

IV. Conclusions

Toward the development of highly sensitive, charging-based active plasmonic devices, we have studied the effects of electron injection in nanorods and nanodisks of various AR and nanoshells of various core VFs and RIs. Using accurate electrodynamics calculations, it is shown that both the nanoparticles' geometry and composition significantly affect their CIPS sensitivities. In nanorods and nanodisks of constant volume, CIPS sensitivity can be increased by using longitudinal and in-plane polarized light respectively, and by choosing higher AR geometries. In nanoshells, the CIPS sensitivities are higher for nanoshells with higher RI and VF of the core. Irrespective of shape and composition, it was shown by quasistatic theory that the CIPS sensitivity of the particles at a particular charging level depends linearly on the resonance position (λ_0) of the uncharged state. This relationship matches with our electrodynamic calculations; from these findings we conclude that nanoparticles with higher λ_0 are more sensitive to CIPS. The particles' CIPS can be further enhanced by increasing the size of the particles or the RI of the surrounding medium.

CIPS in Au Nanoparticles

J. Phys. Chem. C, Vol. 112, No. 19, 2008 **7317**

Supporting Information Available: Material regarding the differences in experimental and Drude dielectric function of gold below and above 500 nm and its effects on extinction spectra. This material is available free of charge via the Internet at http://pubs.acs.org.

References and Notes

(1) Nath, N.; Chilkoti, A. *Anal. Chem.* **2002**, *74*, 504.

(2) West, J. L.; Halas, N. J. *Annu. Rev. Biomed. Eng.* **2003**, *5*, 285.

(3) Sokolov, K.; Follen, M.; Aaron, J.; Pavlova, I.; Malpica, A.; Lotan, R.; Kortum, R. R. *Cancer Res.* **2003**, *63*, 1999.

(4) Yelin, D.; Oron, D.; Thiberge, S.; Moses, E.; Silberberg, Y. *Opt. Express* **2003**, *11*, 1385.

(5) Ozbay, E. *Science* **2006**, *311*, 189.

(6) Krebig, U.; Volmer, M. *Optical Properties of Metal Clusters*; Springer: New York, 1995.

(7) Coronado, E. A.; Schatz, G. C. *J. Chem. Phys.* **2003**, *119*, 3926.

(8) Grand, J.; Lamy de la Chapelle, M.; Bijeon, J. L.; Adam, P.-M.; Vial, A.; Royer, P. *Phys. Rev. B* **2005**, *72*, 033407.

(9) Noguez, C. *J. Phys. Chem. B* **2007**, *111*, 3806.

(10) Sidhaye, D. S.; Kashyap, S.; Sastry, M.; Hotha, S.; Prasad, B. L. V. *Langmuir* **2005**, *21*, 7979.

(11) Park, S. Y.; Lee, J. S.; Georganopoulou, D.; Mirkin, C. A.; Schatz, G. C. *J. Phys. Chem. B* **2006**, *110*, 12673.

(12) Haes, A. J.; Zou, S.; Schatz, G. C.; VanDuyne, R. P. *J. Phys. Chem. B* **2004**, *108*, 109.

(13) Hanarp, P.; Kall, M.; Sutherland, D. S. *J. Phys. Chem. B* **2003**, *107*, 5768.

(14) Tam, F.; Moran, C.; Halas, N. J. *J. Phys. Chem. B* **2004**, *108*, 17290.

(15) Miller, M. M.; Lazarides, A. A. *J. Phys. Chem. B* **2005**, *109*, 21556.

(16) Goad, D. G. W.; Moskovits, M. *J. Appl. Phys.* **1978**, *49*, 2929.

(17) Henglein, A.; Mulvaney, P.; Linnert, T. J. *Faraday Discuss.* **1991**, *92*, 31.

(18) Mulvaney, P. *Langmuir* **1996**, *12*, 788.

(19) Ung, T.; Giersig, M.; Dunstan, D.; Mulvaney, P. *Langmuir* **1997**, *13*, 1773.

(20) Chapman, R.; Mulvaney, P. *Chem. Phys. Lett.* **2001**, *349*, 358.

(21) Toyota, A.; Nakashima, N.; Sagara, T. *J. Electroanal. Chem.* **2004**, *565*, 335.

(22) Baum, T.; Bethell, D.; Brust, M.; Schiffrin, D. J. *Langmuir* **1999**, *15*, 866.

(23) Daniels, J.; Chumanov, G. *J. Electroanal. Chem.* **2005**, *575*, 203.

(24) Perez-Juste, J.; Liz-Marzan, L. M.; Carnie, S.; Chan, D. Y. C.; Mulvaney, P. *Adv. Funct. Mater.* **2004**, *14*, 571.

(25) Yu, Y. Y.; Chang, S. S.; Lee, C. L.; Wang, C. R. C. *J. Phys. Chem. B* **1997**, *101*, 6661.

(26) Link, S.; Mohamed, M. B.; El-Sayed, M. A. *J. Phys. Chem. B* **1999**, *103*, 3073.

(27) Germain, V.; Brioude, A.; Ingert, D.; Pileni, M. P. *J. Chem. Phys.* **2005**, *122*, 124707.

(28) Zhou, H. S.; Honma, I.; Komiyama, H.; Haus, J. W. *Phys. Rev. B* **1994**, *50*, 12052.

(29) Averitt, R. D.; Westcott, S. L.; Halas, N. J. *J. Opt. Soc. Am. B* **1999**, *16*, 1824.

(30) Sau, T. K.; Murphy, C. J. *J. Am. Chem. Soc.* **2004**, *126*, 8648.

(31) Niklasson, G. A.; Bobbert, P. A.; Craighead, H. G. *Nanostruct. Mater.* **1999**, *12*, 725.

(32) Lamprecht, B.; Schider, G.; Lechner, R. T.; Ditlbacher, H.; Krenn, J. R.; Leitner, A.; Aussenegg, F. R. *Phys. Rev. Lett.* **2000**, *84*, 4721.

(33) Grand, J.; Adam, P. M.; Griamault, A. S.; Vial, A.; Lamy de la Chapelle, M.; Bijeon, J. L.; Kostcheev, S.; Royer, P. *Plasmonics* **2006**, *1*, 135.

(34) Jensen, T. R.; Duval, M. L.; Kelly, K. L.; Lazarides, A. A.; Schatz, G. C.; Van Duyne, R. P. *J. Phys. Chem. B* **1999**, *103*, 9846.

(35) Haynes, C. L.; Van Duyne, R. P. *J. Phys. Chem. B* **2001**, *105*, 5599.

(36) Zheng, Y. B.; Juluri, B. K.; Mao, X.; Walker, T. R.; Huang, T. J. *J. Appl. Phys.* **2008**, *103*, 014308.

(37) Malinsky, M. D.; Kelly, K. L.; Schatz, G. C.; Van Duyne, R. P. *J. Am. Chem. Soc.* **2001**, *123*, 1471.

(38) Aizpurua, J.; Hanarp, P.; Sutherland, D. S.; Käll, M.; Bryant, G. W.; García de Abajo, F. J. *Phys. Rev. Lett.* **2003**, *90*, 057401.

(39) Zheng, Y. B.; Huang, T. J.; Desai, A. Y.; Wang, S. J.; Tan, L. K.; Gao, H.; Huan, A. C. H. *Appl. Phys. Lett.* **2007**, *90*, 183117.

(40) Zhang, X.; Hicks, E. M.; Zhao, J.; Schatz, G. C.; Van Duyne, R. P. *Nano Lett.* **2005**, *5*, 1503.

(41) Mulvaney, P.; Pérez-Juste, J.; Giersig, M.; Liz-Marzán, L.; Pecharromán, C. *Plasmonics* **2006**, *1*, 61.

(42) Bohren, C. F.; Huffman, D. R. *Absorption and Scattering of Light by Small Particles*; John Wiley & Sons: New York, 1983.

(43) Yang, W. H.; Schatz, G. C.; Van Duyne, R. P. *J. Chem. Phys.* **1995**, *103*, 869.

(44) Waterman, P. C. *Phys. Rev. D* **1971**, *3*, 825.

(45) Maier, S. A. Ph.D. Thesis; California Institute of Technology: Pasedena, CA, 2003.

(46) Sönnichsen, C. Ph.D. Thesis; Ludwig-Maximilians-Universtät: München, 2001.

(47) Johnson, P. B.; Christy, R. W. *Phys. Rev. B* **1972**, *6*, 4370.

(48) Purcell, E. M.; Pennypacker, C. R. *Astrophys. J.* **1973**, *186*, 705.

(49) Draine, B. T.; Flatau, P. J. *J. Opt. Soc. Am. A* **1994**, *11*, 1491.

(50) Draine, B. T.; Flatau, P. J. *User Guide to the Discrete Dipole Approximation Code DDSCAT 6.1*; 2004.

(51) Goodman, J. J.; Draine, B. T.; Flatau, P. J. *Opt. Lett.* **1991**, *16*, 1198.

(52) Hao, E.; Schatz, G. C. *J. Chem. Phys.* **2004**, *120*, 357.

(53) Jain, P. K.; Lee, K. S.; El-Sayed, I. H.; El-Sayed, M. A. *J. Phys. Chem. B* **2006**, *110*, 7238.

(54) Oldenburg, S. J.; Averitt, R. D.; Westcott, S. L.; Halas, N. J. *Chem. Phys. Lett.* **1998**, *288*, 243.

(55) Prodan, E.; Radloff, C.; Halas, N. J.; Nordlander, P. *Science* **2003**, *302*, 419.

(56) Malinsky, M. D.; Kelly, K. L.; Schatz, G. C.; Van Duyne, R. P. *J. Phys. Chem. B* **2001**, *105*, 2343.

(57) Wang, Z.; Chumanov, G. *Adv. Mater.* **2003**, *15*, 1285.

(58) Novo, C.; Mulvaney, P. *Nano Lett.* **2007**, *7*, 520.